Sub-Surface Flaw Detection of GFRP Components Using Non-Destructive Methods

Saiprasanna Kumar JV, Rahul B, Dharani J

Abstract*: Non-destructive testing enables a way to identify and evaluate the surface as well as sub-surface defects of materials, without altering the structural integrity. This paper concentrates the experimental demonstration on few of the non-destructive techniques. Based on the test results the nature & properties of the defects are discussed in comparison with base material. The glass/epoxy laminates are prepared in the form of pipes & laminates in which artificial defects are introduced by inserts & milled holes. By testing these defective specimens through various methods like ultrasonic testing, radiography testing, thermography testing the defects are identified and hence the properties of the defects are discussed.

***Index Terms*: Non-destructive testing, Glass-Epoxy laminates, Thermography, Radiography, Ultrasonic testing.**

I. INTRODUCTION

Non-destructive testing is an effective methodology to establish the characteristics of the material like internal flaws, surface discontinuities, porosity, de-bond and wall thinning, without affecting the quality and serviceability of the material [1]. It can also be described as a qualification or inspection process to determine the suitability of the material for the intended functioning with reference to some standards. Composite materials are the combination of two or base materials in macroscopic level in order to combine the advantages of the base materials. It has numerous advantages like high strength to weight ratio, increased stiffness, high fatigue strength to bring them as an essential material for various industries especially in aerospace [2].

Numbers of non-destructive techniques are used for the inspection of various materials. The widely used techniques are visual inspection, dye penetrant testing, thermography, ultrasonic testing, and radiography. The defects in the composite material play a significant role in the failure mechanism such as matrix cracking, fiber-breakage, fiber pull-out, delamination and de-bonding depend upon the position, shape, type and size of the damage. So it is essential to select a suitable testing method to localize the damage for the safe and effective service of the material in terms of safety and cost of the test method [3]. Researchers have extended and proved the application of NDT to composite materials effectively [4]. Koyama utilized the eddy current technique to inspect and assess the impact damage of carbon fiber reinforced pressure vessels [5]. Karabutov proved the utilization of the laser spectroscopy for the determination of defects in the CFRP laminates [6]. Tan has used the radiography and computer tomography techniques for the damage assessment of impact loaded stitched composites [7]. Arumugam has described the failure modes of composite structures from the emitted acoustic signal during failure [8]. In this paper the thermographic, radiographic and ultrasonic NDT tests are carried out on the GFRP composites with known defects and the effectiveness of the test methods are evaluated..

II. MATERIALS & FABRICATION METHODS

The laminated plate specimens are prepared with Glass fiber bi-directional fabric (Obtained fron St. Gobain pvt ltd.,) as reinforcement and LY556 (Bought from Sakthi fibers pvt ltd.,) as matrix along with HY 951 as the catalyst. The laminated plates are fabricated through hand lay-up technique and cured in hot air oven with temperature prescribed by the manufacturer. The plates are fabricated in two different dimensions say 150mm*150mm*2.6mm with 12 layers (Plate 1) of fabric and 200mm*200mm*3.8mm (Plate 2) with 18 layers of fabric. Artificial defects are introduced in Plate 1 through two 1mm thick aluminium leaf inserts placed at 2^{nd} and 4^{th} layer of the specimen respectively as shown in Fig. 1(a). In Plate 2 the defects are introduced in the form of Teflon inserts and milled holes where the defects are made in different dimensions. Totally nine Teflon inserts are placed in Plate 2, each one at successive even layers of the specimen say 2^{nd}, 4^{th}, 6^{th}, 8^{th}, 10^{th}, 12^{th}, 14^{th} and 16^{th} layers as shown in Fig. 1(b). For different specimens three different Teflon sheets are selected with geometries as 10mm*10mm*1mm, 15mm*15mm*1mm and 20mm*20mm*1mm. On the other hand, the plate is milled with eight circular holes having depths as 0.2mm, 0.4mm, 0.6mm, 0.8mm, 1mm, 1.2mm, 1.4mm and 1.6mm at different locations on the surface of the plate as shown in Fig. 1(c).

Revised Manuscript Received on May 10 ,2019

Dr. Saiprasanna Kumar JV, Aeronautical Engineering, GKM College of Engineering & Technology, Chennai, India.
Rahul B, Aeronautical Engineering, GKM College of Engineering & Technology, Chennai, India.
Dharani J, Aeronautical Engineering, GKM College of Engineering & Technology, Chennai, India.

(a) (b) (c)

Fig. 1 (a) 150m*150*2.6mm^3 GFRP plate with 1mm thick aluminium leaf insert (b) 200*200*3.8mm^3 GFRP plate with 10*10*1mm^3 teflon insert (c) 200*200*3.8mm^3 GFRP plate with 11mm milled hole

(a) (b)

Fig. 2 10mm thick hollow GFRP pipe with (a) 10*10*1mm^3 teflon inserts (b) 11mm milled hole

For different specimens, the diameter of the milled holes is varied as 9mm, 11mm and 13mm.

The hollow pipe specimens are made with Glass fiber strands through filament winding technique having 75mm internal diameter and 85mm external diameter. As like the plate specimens, the pipe specimens also made with Teflon sheet inserts and milled holes. Three Teflon inserts are placed in the hollow pipes with equal distances from the top to bottom in the longitudinal axis of the pipe as shown in Fig. 2(a). For the different specimens the size of the Teflon inserts are set to vary in three configurations as like the plate. The holes are milled in the hollow pipes as shown in Fig. 2(b) by following the same pattern as the Teflon inserts in the hollow pipes. Hence for different specimens the diameter of the milled holes are made to vary as 9mm, 11mm and 13mm like the milled holes in the Plate2.

III. EXPERIMENTAL METHODS & INSTRUMENTATION

A. Radiography testing

In the radiography testing, the X-rays or Gamma rays are allowed to fall on the material and captured by a receiver which is placed behind the material. By analyzing the density of incident wave in the receiver, the geometry of the defect could be determined. The defects which are perpendicular to the excitation axis will hard to detect [9].

In the Digital radiography testing shown in Fig. 3, the specimen is fitted in rotary module and aligned as required by the controller. The amount of x-rays emitted is controlled by the application of electrical voltage. Amorphous Silicon panel with Cesium-Iodide is used as the detector which converts the falling x-ray density to corresponding voltage which could be analyzed through the software.

The specimens with known artificial defects are tested under controlled x-ray exposure with the application of electrical input to x-ray emitter. The range of the inputs is 85-95kV & 0.8-1.2mA for the duration of 1-3seconds.

B. Thermography testing

In this testing the material is exposed to the thermal excitation and captured by a suitable receiver. By picking the thermal energy fluctuation across the defect will give the positional and geometrical information of the internal as well as the surface defects. Unlike the other testing methods, this could be used for larger areas. The defects having lesser area than the depth could not be detected by this method due to the minimum difference in fluctuation of thermal energy [10].

Fig. 3 X-Ray Radiography test setup

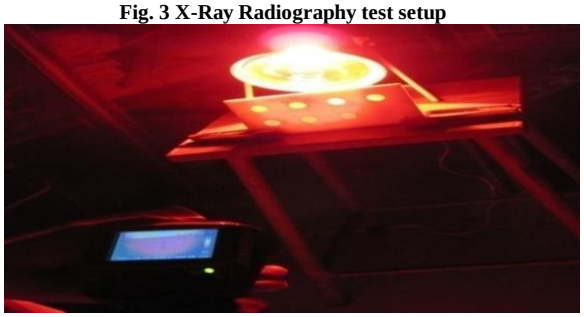

Fig. 4 Thermography test setup

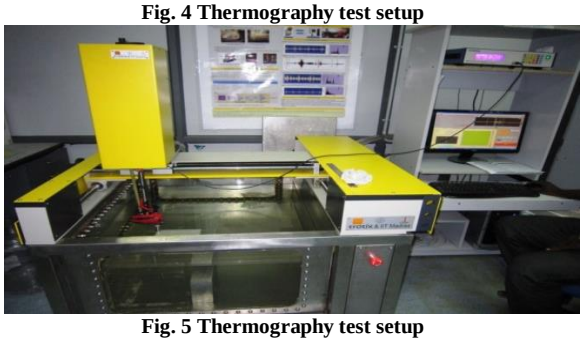

Fig. 5 Thermography test setup

A 150W IR lamp and 1000W halogen lamp are used as the heat sources and un-cooled FLIR is used as the detector for obtaining the heat fluctuations. The change in resistance across the heat fluctuation is measured and processed for the creation of thermal images.

The thermography test shown in Fig. 4, has been done by taking 150W IR lamp for the milled test specimens and 1000W halogen lamp for the specimens with the aluminium, Teflon inserts as the thermal energy source.

C. Ultrasonic testing

Ultrasonic testing analyzes the predictable reflection of high frequency sound waves from the defects through suitable analyzer which are generated at the surface of the specimen. This pulse echo method gives us the qualitative and quantitative information of the both surface and internal flaws [11]. The wave propagation velocity and amplitude are taken as the variables for the detection of defects which are altered by the geometry, absorption and scattering.

Published By:
Blue Eyes Intelligence Engineering
& Sciences Publication

In the ultrasonic testing shown in Fig 5, the specimen is fitted inside the mechanical module contains the coupler typically water to avoid the mismatch of air and specimen. The transducer holder is connected to controller to move it in x and y directions. The transducer is a computer controlled pulse transmitter/receiver. The transceiver analyzes the reception of ultrasonic signals in compare with transmitted and generates the information as A, B & C scan images.

The scanning of ultrasonic testing has done by taking 2-2.25MHz as the frequency, 0.15-0.23mm as the resolution and for the time period of 90-420minutes for various specimens.

IV. RESULTS AND DISCUSSIONS

A. Radiography testing

The adoptive histogram shown in Fig. 6(c), Fig. 7(c), Fig. 8(c), Fig. 9(c) and Fig. 10(c) is more visible for the defects when compared to the ordinary x-ray image shown in Fig. 6(b), Fig. 7(b), Fig. 8(b), Fig. 9(b) & Fig. 10(b) and the sub-surface defects could be identified qualitatively through this technique and the relative position of the defect is also not detectable.

Teflon inserts shown in Fig. 7(a) and Fig. 9(a) are visible clearly even the fabric details also in the adaptive histogram than the ordinary x-ray image and the relative position of the defect is not identified while looking all the inserts are appears to be in the same surface.

The histogram images give us the relative depth of the flaws clearly through the color variation unlike other type defects than the x-ray image. The defects shown in Fig. 9(a) are not visible clearly since inserts were very thin and small for the X-rays to be absorbed and form a contrasting image. For comparison the adoptive histogram is better than the ordinary x-ray.

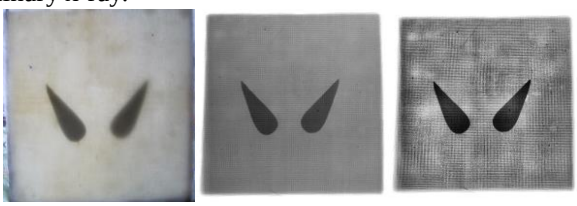

(a) (b) (c)

Fig. 6 Radiographic images of laminate with aluminium inserts (a) Visual (b) Ordinary X-ray (c) Adaptive Histogram

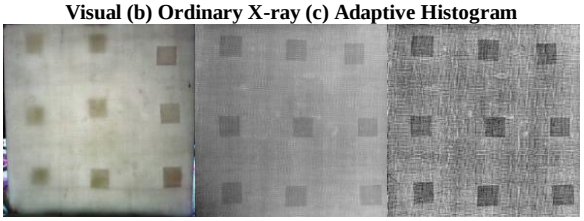

(a) (b) (c)

Fig. 7 Radiographic images of laminate with 10*10*1 mm^3 teflon inserts (a) Visual (b) Ordinary X-ray (c) Adaptive Histogram

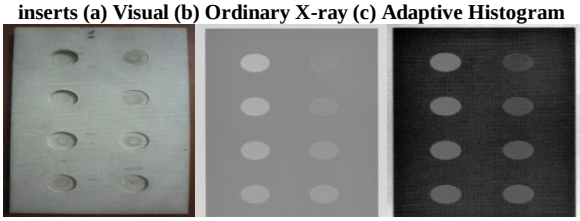

(a) (b) (c)

Fig. 8 Radiographic images of laminate with 9mm milled holes (a) Visual (b) Ordinary X-ray (c) Adaptive Histogram

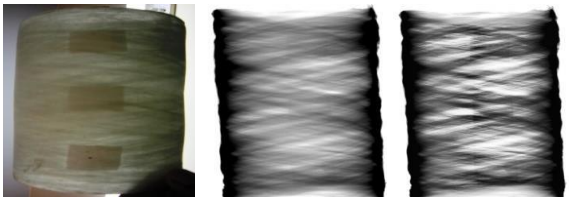

(a) (b) (c)

Fig. 9 Radiographic images of pipe with 10*10*1 mm^3 teflon inserts (a) Visual (b) Ordinary X-ray (c) Adaptive Histogram

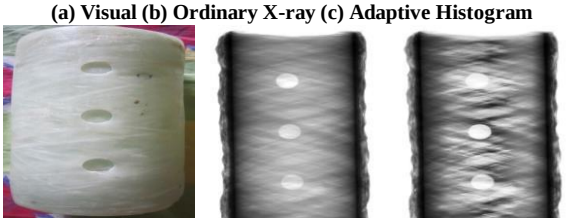

(a) (b) (c)

Fig. 10 Radiographic images of pipe with 9mm milled holes (a) Visual (b) Ordinary X-ray (c) Adaptive Histogram

In Fig. 8 and Fig. 10 the surface flaws are detected and the relative depth of the defect is more visible in the adaptive histogram than the ordinary x-ray image.

B. Thermography testing

From the Fig. 11, it can be analyzed that the area of the insert is brighter since the defect absorbs more heat and from the graph shown in Fig. 12, the insert retain the heat for a longer time ever after the removal of the heat source hence it would be a metal. The upper curve in the Fig. 12 shows higher temperature than the lower hence it shows the upper curve denotes the insert which closer to the heat source.

The Teflon at the upper layers appears more clearly in the thermal image shown in Fig. 13 than the teflons at the lower layer due to the distance from the heat source. Even also there is some notable difference for the teflons at the lower layer than the surface due the variation of thermal properties between that. The decrement in the all these curves shown in Fig. 14 after peak says the defect is either a gap or some other material with moreover similar properties like the surface and it is evident from the curves of surface temperature & innermost Teflon temperature.

In the Fig. 15, the deepest hole appears more clearly than the others and surface hence it gives the relative depth of the defect. From the deepest hole has the higher temperature than the others and the lightest hole has the temperature merely similar to the surface.

The hotspot present in the thermographic image shows that there is some defect because of the thermal energy absorption. Also it could be absorbed from the temperature variation curves also.

The thermographic images shows that the depth of the flow is very less when compared to the specimen thickness through minute temperature variation. Even the flaw also could be detected from the temperature variation curves from the temperature difference between the flaw and surface.

Published By:
Blue Eyes Intelligence Engineering
& Sciences Publication

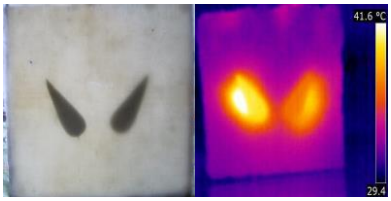

(a) (b)

Fig. 11 Thermographic images of laminate with aluminium inserts (a) Visual (b) Thermography

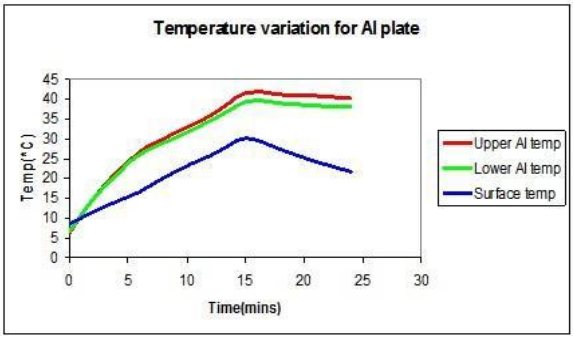

Fig. 12 Temperature variation at interest point of laminate with aluminium inserts

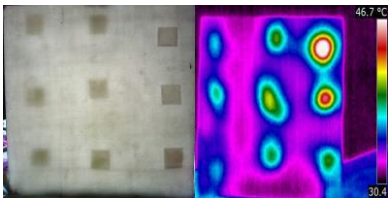

(a) (b)

Fig. 13 Thermographic images of laminate with 10*10*1mm^3 teflon inserts (a) Visual (b) Thermography

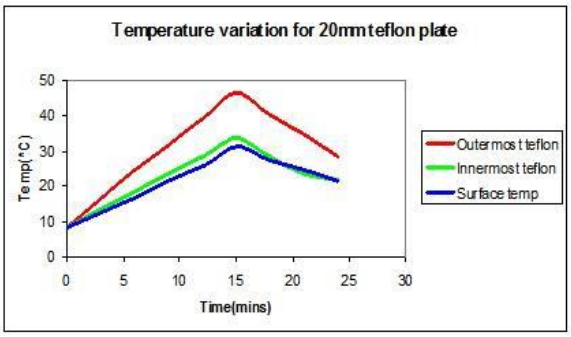

Fig. 14 Temperature variation at interest point of laminate with 10*10*1mm^3 teflon inserts

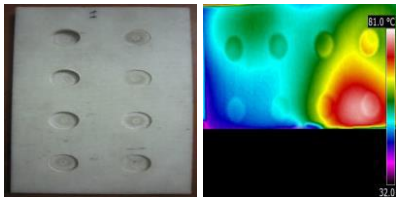

(a) (b)

Fig. 15 Thermographic images of pipe with 9mm milled holes (a) Visual (b) Thermography

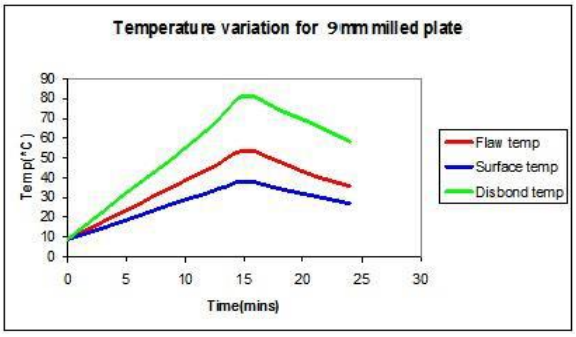

Fig. 16 Temperature variation at interest point of pipe with 9mm milled holes

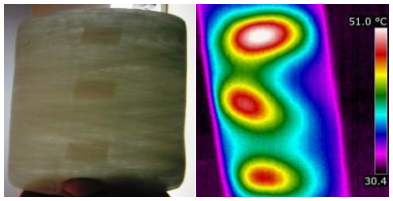

(a) (b)

Fig. 17 Thermographic images of pipe with 10*10*1mm^3 teflon inserts (a) Visual (b) Thermography

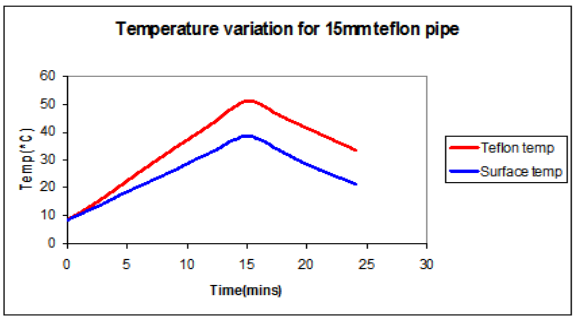

Fig. 18 Temperature variation at interest point of pipe with 10*10*1mm^3 teflon inserts

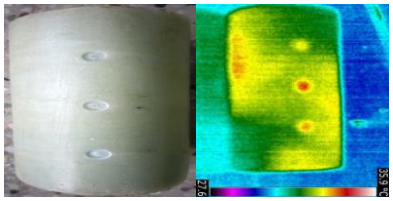

(a) (b)

Fig. 19 Thermographic images of pipe with 9mm milled holes (a) Visual (b) Thermography

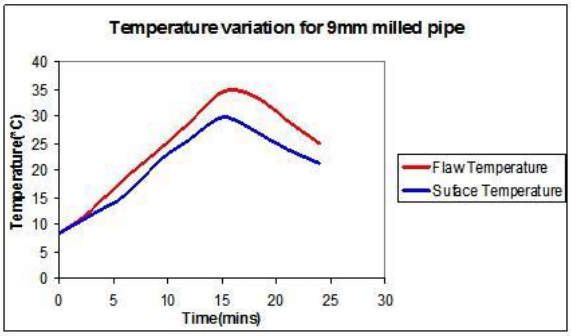

Fig. 20 Temperature variation at interest point of pipe with 9mm milled holes

C. Ultrasonic testing

From the observation of Fig. 21(d) and Fig. 22(d), A-scan at different places of the specimen shows that the front wall remains same and back wall differs with respect to the point of detection where there is defect or not. From the value of amplitude and its occurring point with respect to the time one could identify the defect also its properties.

B-scan shown in Fig. 21(c) and Fig. 22(c) gives an idea about the placement of the inserts. The fabric on the top surface is represented by the green colored band and the white color band represents the resin layer. The image shows that the resin layer is very thick. The dark blue color represents the fiber layers preceding the top layers. The green colored band in between represents the inserts. The inserts are shown in the same color as that of the front wall because; its density was comparably higher than that of the fabric.

From the Fig. 21(b) and Fig. 22(b) of C-scan images shows from the intense contrast, first insert (on the right) has represents that the insert is nearer to the surface. The second insert (on the left) doesn't have a bright contrast compared to the first & thus indicates that it is positioned deeper in the laminate.

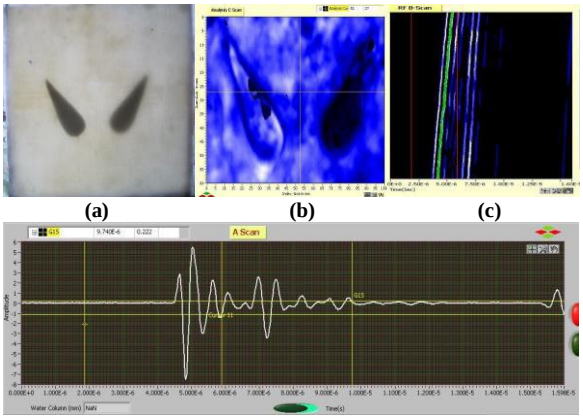

(a) (b) (c)

(d)

Fig. 21 Ultrasonic images of laminate with aluminium inserts in the region without any insert (a) Visual (b) C-Scan (c) B-Scan (d) A-Scan

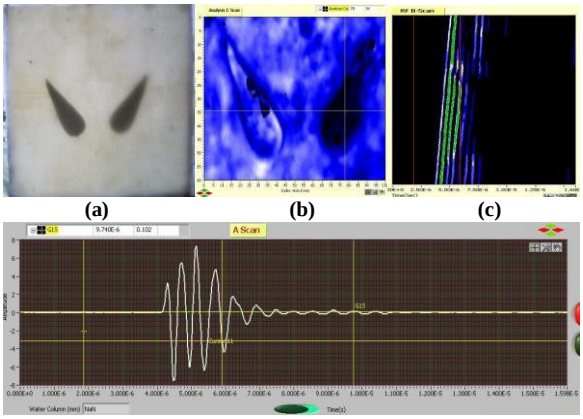

(a) (b) (c)

(d)

Fig. 22 Ultrasonic images of laminates with aluminium inserts in the region of upper insert (a) Visual (b) C-Scan (c) B-Scan (d) A-Scan

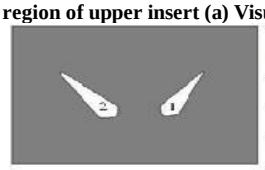

Flaw number	ΔT E-6 (sec)	D (mm)
1	1.05	1.37
2	2	2.6
Laminate	2.4	3.12

Fig. 23 Flaw depth in laminates with aluminium inserts

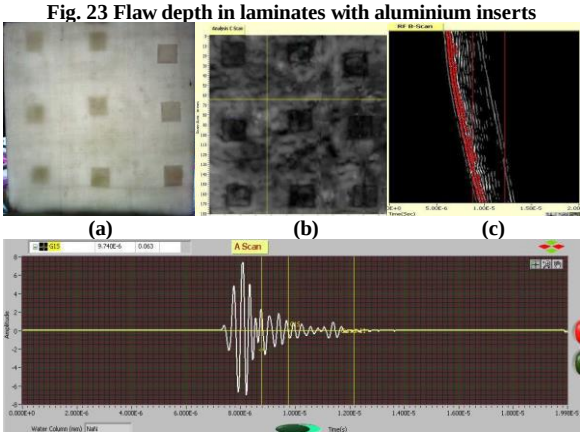

(a) (b) (c)

(d)

Fig. 24 Ultrasonic images of laminate with 10*10*1mm^3 teflon inserts in the region without any insert (a) Visual (b) C-Scan (c) BScan (d) A-Scan

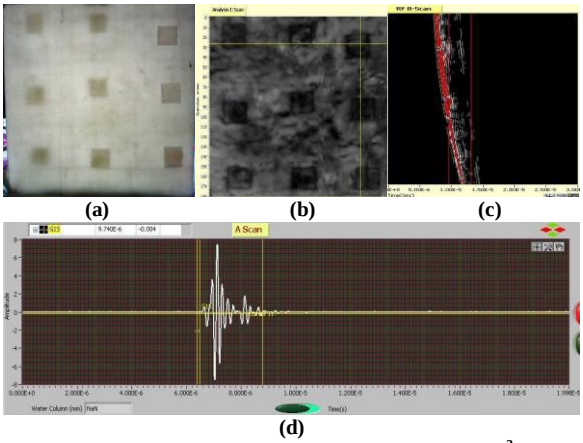

(a) (b) (c)

(d)

Fig. 25 Ultrasonic images of laminate with 10*10*1mm^3 teflon inserts in the region of upper most insert (a) Visual (b) C-Scan (c) B-Scan (d) A-Scan

So this image cannot clearly represent flaws or inserts at a larger depth in a thick specimen but by adjusting the resolution, thicker sections can be better imaged. It also shows that the specimen has many other defects which were caused during its fabrication.

In the A-scan of laminates with Teflon inserts shown in Fig. 24(d) and Fig. 25(d), the spacing between front wall and back wall signals reduce as we move up from the lowermost Teflon to uppermost Teflon indicating that the inserts are placed at various depths inside the laminate, so an idea about their relative depth is obtained. The position of front wall is somewhat constant at various locations on the laminate, indicating that the thickness of the laminate is same throughout.

In the B-scan image shown in Fig. 24(c) and Fig. 25(c), the red colored band represents the upper fabric layers. The region of Teflon is shown as a blackened region along a continuous grey colored band, since Teflon's thickness low compared to that of fabric. Else it would've shown up in a different color. The white color in certain places may be due to excess resin concentrated at that region or it may be due to excess wetting of the fabric layer. Since the red colored band is continuous, it shows that flaws are not on the surface.

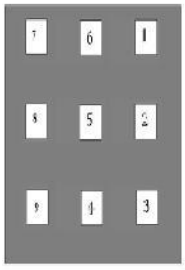

Flaw number	ΔT E-6 (sec)	D (mm)
1	0.36	0.468
2	0.74	0.962
3	1.09	1.417
4	1.46	1.99
5	1.83	2.379
6	2.18	2.834
7	2.55	3.315
8	2.88	3.744
9	3.10	4.03
Laminate	3.4	4.42

Fig. 26 Flaw depth in laminate with with 10*10*1mm^3 teflon Inserts

Published By:
Blue Eyes Intelligence Engineering
& Sciences Publication

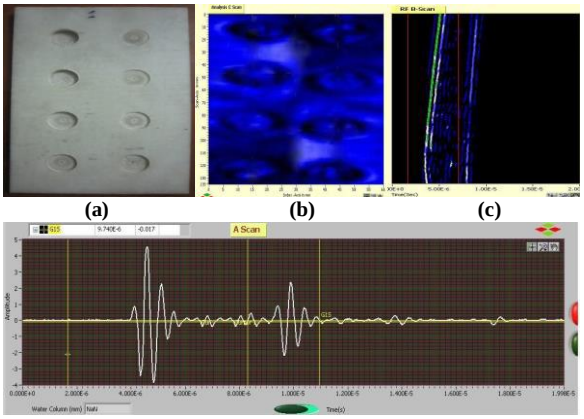

Fig. 27 Ultrasonic images of laminate with 9mm milled holes in the region without defect (a) Visual (b) C-Scan (c) B-Scan (d) A-Scan

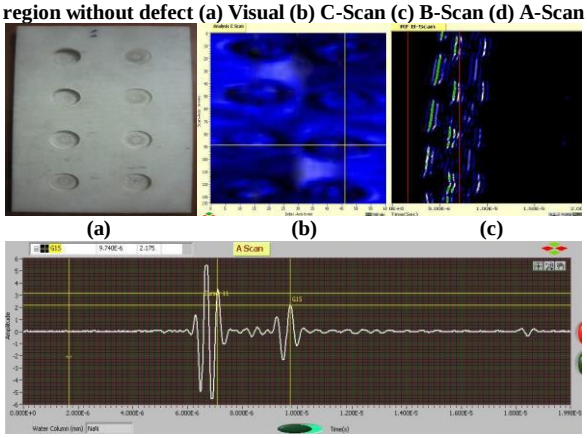

Fig. 28 Ultrasonic images of laminates with 9mm milled holes in the 1.2mm depth hole region (a) Visual (b) C-Scan (c) B-Scan (d) A-Scan

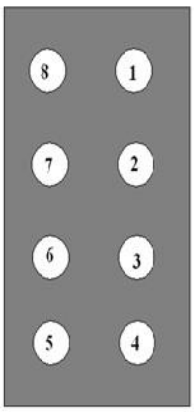

Flaw number	ΔT e-6 (sec)	D (mm) [5.33-D]
1	3.72	0.49
2	3.33	0.99
3	2.95	1.5
4	2.56	1.98
5	2.18	2.49
6	1.79	3.003
7	1.41	3.497
8	1.02	3.99
Laminate	4.1	5.33

Fig. 29 Flaw depth in laminates 9mm milled holes

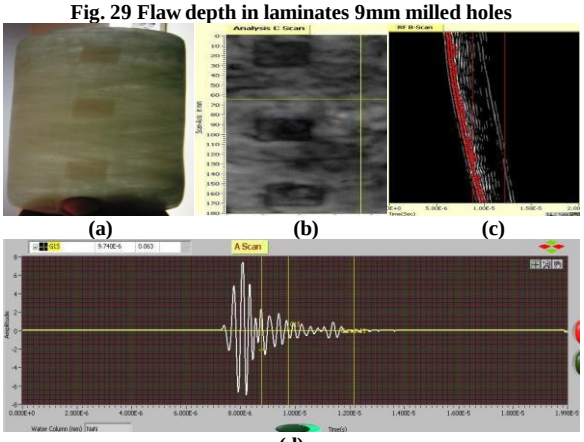

Fig. 30 Ultrasonic images of pipes with 10*10*1mm^3 teflon inserts in the region of without insert (a) Visual (b) C-Scan (c) B-Scan (d) A-Scan

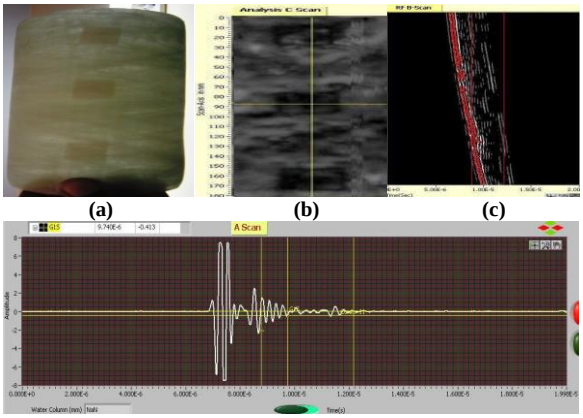

Fig. 31 Ultrasonic images of pipes with 10*10*1mm^3 teflon inserts in the region of middle insert (a) Visual (b) C-Scan (c) B-Scan (d) A-Scan

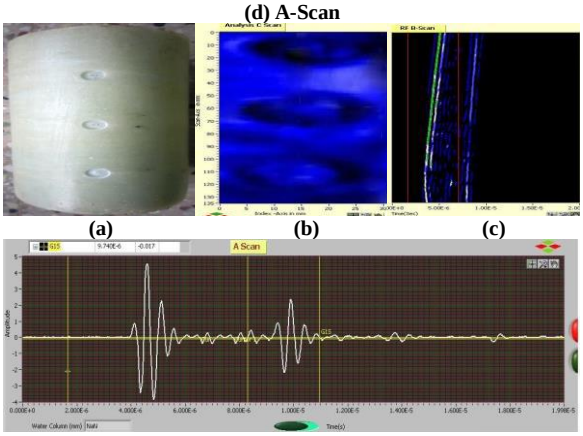

Fig. 32 Ultrasonic images of pipes with 9mm milled holes in the region Without any defect (a) Visual (b) C-Scan (c) B-Scan (d) A-Scan

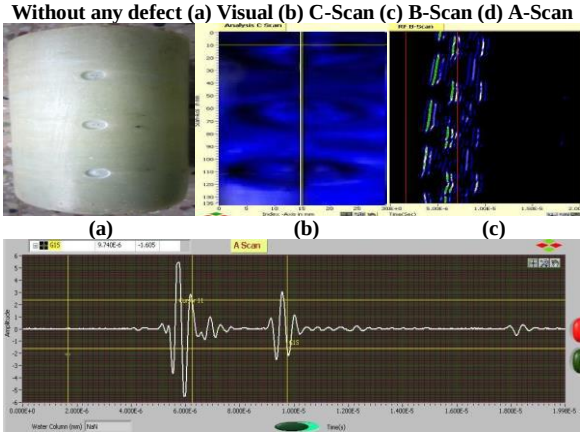

Fig. 33 Ultrasonic images of pipes with 9mm milled holes in the region of deepest defect (a) Visual (b) C-Scan (c) B-Scan (d) A-Scan

In the C-scan shown in Fig. 24(b) and Fig. 25(b), various inserts at a minor depth difference can be easily visualized although it cannot be said as to which one is at top layer and which one is at bottom. But this image eases the determination of insert depth and location by moving the cursor to various insert positions and analyzing its corresponding A & B scans. The image shows that the specimen has many other defects which were caused during its fabrication.

The front wall also varies in this case unlike others due to the milled defects and this could be analyzed through the amplitude variation of A-scan image shown in Fig. 27(d) and Fig. 28(d).

The respective color bands represents there is no material up to the fabric layer in the milled space is indicated by the darker region and followed by blue and white represents the fabric as well as the matrix. The black colored band in between is not because of a void, but it is a separation shown after every 2mm of scanning.

The C-scan image given in Fig. 27(b) and 28(b) shows, the position of defects and also indicates the test points where the further processing to be done for the estimation of properties of the defects.

V. CONCLUSION

The fabricated GFRP specimens are tested with various NDT methods to characterize the induced defects. Radiographic method can detect surface & sub-surface flaws in quick time and its dimensions are not known. For deep surface flaws it's not known whether the flaw runs through the thickness of the specimen or not. It's very difficult to analyze thin specimens sidewise and multiple flaws one below the other are difficult to analyze in single image. Thermography was successful in detecting local variations in thermal diffusivity arising from in-homogeneities in the composite material. In addition to induced flaws, flaws due to improper fabrication were also revealed and this method is not suitable for thicker sections. Thin sections with very thin and small induced flaws were not properly detected and possible to verify the relative depth of flaws inside the laminate. In the A-scan amplitude of the signals doesn't say anything like density, dimension and thickness of the defects. It can also be said whether the scanned specimen has a uniform thickness throughout or not and requires very close monitoring to identify the presence of flaws. B-scan shows the relative depth of flaws and also thickness/density of the flaw. It is also possible to detect the flaws induced due to improper fabrication of laminate and not possible to identify the flaw geometry. The C-scan allows identifying the surface and sub-surface flaws to a decent depth in a single plane but they cannot be differentiated. A rough idea about flaw geometry is obtained and the presence of surface irregularities can be seen.

REFERENCES

1. C. D. Lockard, "Anomaly detection in radiographic images of composite materials via crosshatch regression", *ProQuest Dissertations & Theses Global database*, 2015.
2. B. Xu B and H. Y. Li, "Advanced composite materials and manufacturing engineering", *International Conference of Advance Composite Materials and Manufacturing Engineering*, 2012.
3. A. Katunin, M. Danczak and P. Kostka, "Automated identification and classification of internal defects in composite structures using computed tomography and 3D wavelet analysis", *Archives of Civil and Mechanical Engineering"*, Vol. 5(2), 2015, pp. 436-448.
4. G. Garney, "Defects found through non-destructive testing methods of fiber reinforced polymeric composites", *ProQuest Dissertations & Theses Global database*, 2006.
5. K. Koyama, H. Hoshikawa and G. Kojima, "Eddy Current Nondestructive Testing for Carbon Fiber- Reinforced Composite", *Journal of Pressure Vessel Technology*, Vol. 135(4), 2013, pp. 1-5.
6. A. A. Karabutov and N. B. Podymova, "Quantitative analysis of the influence of voids and delaminations on acoustic attenuation in CFRP composites by the laser-ultrasonic spectroscopy method", *Composites Part B: Engineering*, Vol. 56(0), 2014, pp. 238-244.
7. K. T. Tan, N. Watanabe and Y. Iwahori, "X-ray radiography and micro-computed tomography examination of damage characteristics in stitched composites subjected to impact loading", *Composites Part B: Engineering*, Vol. 42(4), 2011, pp. 874-884.
8. V. Arumugam, C. S. Kumar, C. Santulli, F. Sarasini and A. J. Stanley, "A Global Method for the Identification of Failure Modes in Fiberglass Using Acoustic Emission", *Journal of Testing and Evaluation*, Vol. 39(5), 2011, pp. 954-966.
9. W. S. Burkle and L. P. Lemle, "The Effect of Order-of-Film Placement in Composite Film Radiography," *Materials Evaluation*, Vol. 51(3), 1993, pp. 327-329.
10. R. Mulaveesalaa and S. Tuli, "Applications of Frequency Modulated Thermal Wave Imaging For Non-destructive Characterization," Materials Evaluation, Vol. 63(10), 2005, pp. 1046-1050.
11. I. Oguma, R. Goto and T. Sugiura, "Ultrasonic inspection of an internal flaw in a ferromagnetic specimen using angle beam EMATs," *Przeglad Elektrotechniczny*, Vol.88(7B), 2012, pp. 78-81.

AUTHORS PROFILE

Dr. J. V. Saiprasanna Kumar graduated from IIT Madras and pursued Ph.D in Anna University. He is interested to doing research in Non Destructive Testing, Composite Materials and Material Characterization.

Rahul B completed his U.G in Aeronautical Engineering at Tagore Engineering College and P.G in Avionics at MIT Campus. His primary research areas are Composite materials and Unmanned Aerial Vehicles.

Dharani J has done her U.G in Aeronautical Engineering at PMR Engineering College and P.G in Aeronautical Engineering at MIT Campus. She interested to doing in Numerical techniques and Image processing.